東北大学機関リポジトリ
TOUR
Tohoku University Repository

Superselective Drug Delivery Using Doxorubicin-Encapsulated Liposomes and Ultrasound in a Mouse Model of Lung Metastasis Activation

著者	Tomoki Ouchi, Ariunbuyan Sukhbaatar, Sachiko Horie, Maya Sakamoto, Kiyoto Shiga, Shiro Mori, Tetsuya Kodama
journal or publication title	Ultrasound in Medicine & Biology
volume	44
number	8
page range	1818-1827
year	2018-05-21
URL	http://hdl.handle.net/10097/00135336

doi: 10.1016/j.ultrasmedbio.2018.04.003

Creative Commons : 表示 - 非営利 - 改変禁止
http://creativecommons.org/licenses/by-nc-nd/3.0/deed.ja

Superselective drug delivery using doxorubicin-encapsulated liposomes and ultrasound in a mouse model of lung metastasis activation

Tomoki Ouchi[1,2], Ariunbuyan Sukhbaatar[1,2,3], Sachiko Horie[1,2],
Maya Sakamoto[4], Kiyoto Shiga[5], Shiro Mori[1,2,6], Tetsuya Kodama[1,2]

[1] Laboratory of Biomedical Engineering for Cancer, Graduate School of Biomedical Engineering, Tohoku University, 4-1 Seiryo, Aoba, Sendai, Miyagi 980-8575, Japan

[2] Biomedical Engineering Cancer Research Center, Graduate School of Biomedical Engineering, Tohoku University, 4-1 Seiryo, Aoba, Sendai, Miyagi 980-8575, Japan.

[3] Graduate School of Dentistry, Tohoku University, 4-1 Seiryo, Aoba, Sendai, Miyagi 980-8575, Japan

[4] Department of Oral Diagnosis, Tohoku University Hospital, 1-1 Seiryo, Aoba, Sendai, Miyagi 980-8574, Japan

[5] Department of Head and Neck Surgery, Iwate Medical School, 19-1 Uchimaru, Morioka, Iwate 020-8505, Japan

[6] Department of Oral and Maxillofacial Surgery, Tohoku University Hospital, 1-1 Seiryo, Aoba, Sendai, Miyagi 980-8575, Japan

Corresponding author:

Tetsuya Kodama, PhD (Eng.), PhD (Med.)

Laboratory of Biomedical Engineering for Cancer,

1 Graduate School of Biomedical Engineering, Tohoku University,

2 4-1 Seiryo, Aoba, Sendai, Miyagi 980-8575, Japan.

3 **E-mail:** kodama@tohoku.ac.jp; **Phone & Fax:** +81-22-717-7583

Abstract

Conventional treatment of lymph node metastasis involves dissection of the tumor and regional lymph nodes, but this may cause activation of latent metastatic tumor cells. However, there are few reports in animal models regarding the activation of latent metastatic tumor cells and effective methods of treating activated tumor cells. Here, we report the use of a superselective drug delivery system in a mouse model of lung metastasis to treat activated tumor cells with doxorubicin-encapsulated liposomes (DOX-LP) and ultrasound. The axillary lymph node was injected with DOX-LP and exposed to ultrasound so that the released DOX would be delivered from the axillary lymph node to the metastatic lung via the subclavian vein, heart and pulmonary artery. The size of the DOX-LP was optimized to a diameter of 460 nm using indocyanine green-encapsulated liposomes, and the ultrasound intensity was 0.5 W/cm^2. We found that the superselective drug delivery system was effective in the treatment of metastasis in both the lung and axillary lymph node, compared to DOX or DOX-LP alone. We anticipate that this superselective drug delivery system will be a starting point for the development of new techniques for treating lung metastasis in the clinical setting. Furthermore, the superselective drug delivery system may be used to screen novel drugs for the treatment of lung cancer and investigate the mechanisms of tumor cell activation after resection of a primary tumor or lymph nodes.

Key words: doxorubicin; liposomes; ultrasound; lung metastasis; drug delivery system

Introduction

Excision of a primary tumor is beneficial for the local control of cancer, but this procedure risks the promotion of metastasis via homeostatic mechanisms (Demicheli, et al. 2008). In breast cancer (Tagliabue, et al. 2003), head and neck cancer (Sano, et al. 2013), lung cancer (Maniwa, et al. 1998) and other tumors, tumor activation and rapid growth after resection of the primary lesion have been confirmed by clinical (Braunschweiger, et al. 1982) and animal experiments (Fisher, et al. 1989, Van Dierendonck, et al. 1991). Lymph node (LN) dissection is recommended in many cancer therapy guidelines, but this can induce the activation of latent tumor in distant organs (White, et al. 2002). However, there is a paucity of data on the activation of tumor cells in distant organs caused by LN dissection, mainly due to the lack of suitable animal models. Our research group has developed a mouse model of lung metastasis activation using MXH10/Mo-*lpr*/*lpr* (MXH10/Mo/lpr) mice (Shao, et al. 2015). In this model, tumor cells are inoculated into the subiliac LN (SiLN) so that they are delivered to the proper axillary LN (PALN) via lymphatic vessels and to the lung via blood vessels. Metastatic tumor cells in the PALN continue to grow after resection of the SiLN, and the probability of metastasis to the lung is increased in the interval between SiLN inoculation and resection. In the present study, we report the use of a novel, superselective drug delivery system to treat lung metastasis in our mouse model using doxorubicin-encapsulated liposomes (DOX-LP) and ultrasound (US). The metastatic PALN was injected with DOX-LP and then exposed to US. The released DOX was delivered from the PALN to the lung via the subclavian vein, heart and pulmonary artery. It was found that the superselective drug delivery system was very effective at treating metastasis in the lung as well as in the PALN, as

compared to DOX or DOX-LP alone.

Materials and Methods

All *in vivo* protocols were approved by the Institutional Animal Care and Use Committee of Tohoku University.

Mice

MXH10/Mo/lpr mice (16–18 weeks) were bred under specific pathogen-free conditions in the Animal Research Institute, Graduate School of Medicine, Tohoku University (Shao, et al. 2013). Figure 1A shows an anatomical drawing illustrating the features of the lymphatic and venous systems in an MXH10/Mo/lpr mouse (Takeda, et al. 2017). The efferent lymphatic vessel of the PALN is connected to the subclavian vein (Shao, et al. 2013). The thoracoepigastric vein runs adjacent to the SiLN and PALN and connects to the inferior vena cava and subclavian vein.

Preparation of indocyanine green (ICG)- and doxorubicin-encapsulated liposomes

Preparation of a thin lipid film and encapsulation of ICG were carried out as described previously (Mikada, et al. 2017, Miura, et al. 2016). The composition of the lipid film was 1,2-distearoyl-sn-glycero-3-phosphatidylcholine (DSPC; MC8080, NOF Co., Tokyo, Japan) and 1,2-distearoyl-sn-glycerol-3-phosphatidylethanolamine-methoxy-polyethylenglycol (DSPE-PEG[2000-OMe]; DSPE-020CN, NOF Co.) in a ratio of 94:6 mol/mol. ICG-encapsulated liposomes of differing sizes (ICG-LP1 and ICG-LP2) were made

using a freeze-thaw method (Mikada, et al. 2017). The particle size and zeta potential of the ICG-encapsulated liposomes (ICG-LP1 or ICG-LP2) were measured using a dynamic light-scattering method (ELS-Z2, Otsuka Electronics, Tokyo, Japan). The physicochemical characteristics of ICG-LP1 and ICG-LP2 are shown in Table 1. DOX-LP was prepared by the remote loading method (Fritze, et al. 2006, Matsuki, et al. 2017). The composition of the lipid film was the same as that for ICG-LP1 and ICG-LP2. The efficiency of DOX encapsulation was determined by spectrophotometry at 480 nm (SpectraMax2Me, Molecular Devices, Sunnyvale, CA, USA). The physicochemical characteristics of DOX-LP are listed in Table 1.

ICG and DOX release characteristics from liposomes

ICG-LP with a diameter of 320 nm was prepared by the same method described above. ICG-LP or DOX-LP was pre-dispensed into tubes (200 μL per tube). Individual tubes were incubated at 37°C in a water bath (SB-1000, Tokyo Rika Kikai Co., Tokyo, Japan) for 0 h, 1 h, 6 h, 24 h and 48 h. After incubation, each sample was filtered through PD-10 column (GE Healthcare, *Little* Chalfont, UK) to separate released ICG (or DOX) and liposome. Each filtered sample was added with 10 μL of surfactant (Tween20, Wako, Osaka, Japan), incubated in a water bath at 65°C, and sonicated for 1 min (3 times) (2510J-DTH, Yamato Scientific Co., Tokyo, Japan). The absorbance of each tube was measured at 800 nm for ICG and at 480 nm for DOX by spectrophotometry (SpectraMax2Me, Molecular Devices, USA). The release characteristics of ICG-LP and DOX-LP are shown in Appendix Fig. A.1. Both ICG-LP and DOX-LP had similar release characteristics.

ICG distribution into the PALN detected by fluorescence imaging

Fifteen mice were divided into five groups for evaluation of the ICG distribution: ICG alone (n = 3); ICG-LP1 (n = 3); ICG-LP2 (n = 3); ICG-LP2+US (n = 3; spatial-peak temporal-average intensity [I_{SPTA}] = 2.95 W/cm^2); and ICG-LP2+US (n = 3; I_{SPTA} = 0.48 W/cm^2). The US conditions were: frequency, 1-MHz duty ratio; 20%; and exposure time, 60 sec (Kato, et al. 2015, Kato, et al. 2015, Kodama, et al. 2006). ICG-LP1 or ICG-LP2 was directly injected into the PALN, through a 27-G butterfly needle connected to a syringe pump, at a rate of 50 μL/min for 2 min. The PALN was exposed to US 30 min after injection. The biodistribution of ICG-LP1 or ICG-LP2 was detected with an *in vivo* bioluminescence imaging system (IVIS; Xenogen, Alameda, CA, USA) at 0 min, 5 min, 30 min, 1 h, 3 h, 6 h, 24 h and 48 h after injection. After the 48-h measurement, the mice were sacrificed, and the spleen, kidneys, liver, lungs, heart, PALN and SiLN were removed for *ex vivo* fluorescence measurement using the IVIS.

Cell culture

KM-Luc/GFP malignant fibrous histiocytoma-like cells, stably expressing a fusion of the luciferase (Luc) and enhanced green fluorescent protein (EGFP) genes (Li, et al. 2013), were used. Cells were cultured in Dulbecco's Modified Eagle Medium (Sigma-Aldrich, St. Louis, MO, USA) supplemented with 10% fetal bovine serum containing 1% L-glutamine-penicillin-streptomycin and 1% geneticin (G418; Sigma-Aldrich).

Induction of metastasis in the PALN and lung

The concentration of DOX encapsulated in the liposomes was 1.25 mg/kg. Mice were anesthetized by inhalation of a mixture of 2% isoflurane and oxygen. A small incision in the skin over the SiLN was made to expose the surface of the SiLN. The area between the SiLN and PALN was clamped (DDP-09-151 clamp, Daddy D Pro, Sialkot, Pakistan) to prevent flow from the SiLN to the PALN via lymphatic vessels and the thoracoepigastric vein. Cells (1.0×10^6 cells/mL) passaged three times were suspended in a mixture of 20 μL phosphate-buffered saline (PBS) and 40 μL of 400 mg/mL Matrigel (Collaborative Biomedical Products, Bedford, MA, USA) to obtain a concentration of 3.3×10^5 cells/mL. Using a syringe and needle, cells were manually injected into the middle of the SiLN through an incision. The needle was kept in place for 5 min to prevent leakage of the cell solution from the SiLN. After removing the needle and taking off the clamp, the surgical area was thoroughly washed with 20 mL of saline (37°C) to remove any tumor cells that had leaked from the SiLN. The skin wound was closed with 5-0 polyamide-interrupted sutures (Fig. 1B).

Delivery of DOX-LP to the lung via the PALN, and activation of metastatic tumor cells in the lung

Sixteen mice were divided into four groups for evaluation of anti-tumor effects: non-administration (n = 4), DOX alone (n = 4), DOX-LP alone (n = 4) and DOX-LP+US (n = 4). At 6 h post-inoculation of tumor cells, mice were anesthetized by inhalation of a mixture of 2% isoflurane and oxygen. DOX alone or DOX-LP was injected into the PALN under US guidance (25-MHz transducer; VEVO770, Visual Sonics, Toronto, Canada) at a rate of 50 μL/min using a syringe pump. Then, the

PALN was exposed to 1-MHz US (diameter, 12 mm; Honda Electronics, Toyohashi, Japan). Signals at 1.0 MHz were generated by a multifunction synthesizer (WF1946A, NF, Yokohama, Japan) and amplified using a high-speed bipolar amplifier (HSA4101, NF). The I_{SPTA} was set at 0.48 W/cm^2, the duty cycle at 20%, the number of pulses at 200 and the exposure time at 60 sec. It has been reported that an intensity of 0.48 W/cm^2 does not induce severe adverse effects in LNs (Kato, et al. 2015) (Fig. 1C). To active metastatic cells in the lung, the SiLN was resected with a bipolar coagulator (Erbotom VI050C, Erbe Elektromedizin GmbH, Tübingen, Germany) and surgical microscope (Leica M80, Leica Microsystems GmbH, Wetzlar, Germany). After excision of the SiLN, the surgical area was thoroughly washed with 20 mL of saline (37°C) to remove any tumor cells that had leaked from the tumor-bearing SiLN. The skin wound was closed with 5-0 polyamide-interrupted sutures. The entire resection procedure was accomplished within 10–15 min (Shao, et al. 2015) (Fig. 1D).

Evaluation of anti-tumor effects on lung metastasis

Luciferase activity in the PALN and lung were measured after 6 h and on days 3, 6 and 9 (the day of inoculation being defined as day 0) using the IVIS. The luciferase activity recorded in each group was normalized to that determined at 6 h in the non-administration group.

Histological analysis

The lungs and PALN were harvested on day 9. All harvested samples were fixed in 10% formaldehyde in PBS for 4 days at 4°C (Rapid Fixative; Kojima Chemical

Industry, Inc., Saitama, Japan), dehydrated and then embedded in paraffin. The embedded specimens were cut into 2–4 μm serial sections and either stained with hematoxylin and eosin (HE) or immunostained for detection of CD31-positive cells as previously described (9). The specimen boundary was determined under low magnification using a microscope (BX51; Olympus Corp., Tokyo, Japan) connected to a digital camera (DP72; Olympus Corp.) (Li, et al. 2013).

Statistical analysis

Data are expressed as the mean ± standard deviation (SD), unless otherwise indicated. Statistical comparisons were made using the Mann-Whitney U-test or a Bonferroni post hoc test. Values of $P < 0.05$ were considered to be indicative of statistical significance.

Results

The aim of the present study was to treat metastasis in the PALN and lungs by injecting DOX-LP into the PALN and then exposing the PALN to US. First, we used ICG-LP1 ($n = 3$) and ICG-LP2 ($n = 3$) to determine the effect of liposome size on liposome retention in a LN (Fig. 2A). ICG solution ($n = 3$) was used as the control. ICG solution, ICG-LP1 and ICG-LP2 were injected into the PALN at a rate of 50 μL/min for 2 min. ICG solution spread into the abdominal and thoracic area from the PALN about 30 min after injection, and a fraction of the ICG solution was shown to accumulate in the liver. The fluorescence intensity in the PALN decreased to low levels at 24 h and 48 h after the injection. ICG-LP1 also spread from the PALN 30 min after the injection, and the fluorescence intensity in the PALN fell to low levels

at 24 h and 48 h after injection. By contrast, ICG-LP2 was retained in the PALN for 1 h after the injection. Strong fluorescence intensity was detected in the PALN at 48 h, as compared with that observed for ICG solution and ICG-LP1. Since ICG-LP2 showed higher retention than ICG-LP1, we next determined whether US would effectively release ICG from ICG-LP2 (Fig. 2B). The US intensity (I_{SPTA}) was set at 2.95 W/cm^2 or 0.48 W/cm^2, and the PALN was exposed to US 30 min after the injection of ICG-LP2 into the PALN. Figure 2C shows the fluorescence intensity of ICG in the PALN over time, as illustrated in Fig. 2A and Fig. 2B. For ICG and ICG-LP1, the fluorescence intensity reached a peak 1 h after injection and then immediately decreased. ICG-LP2 reached a peak intensity 3 h after injection. The intensity of ICG-LP2 decreased rapidly after exposure to either US intensity (2.95 W/cm^2 or 0.48 W/cm^2), and there was no significant difference between the two US intensities in ICG retention at 48 h after injection.

Next, we investigated the biodistribution and retention of ICG by making *ex vivo* fluorescence intensity measurements (Fig. 3). Accumulation of ICG in the liver was greater for ICG, ICG-LP1 and ICG-LP2 than for ICG-LP2+US (0.48 W/cm^2 or 2.98 W/cm^2), while ICG retention in the PALN was better for ICG-LP2+US (0.48 W/cm^2 or 2.98 W/cm^2) than for ICG, ICG-LP1 and ICG-LP2. ICG retention in the PALN was greater at an US intensity of 0.48 W/cm^2 than at 2.95 W/cm^2.

Subsequent experiments investigating the treatment of activated lung metastasis utilized an US intensity of 0.48 W/cm^2, DOX-LP (466.8 nm ± 44.3 nm) with a similar size to ICG-LP2 (462.3 ± 87.6 nm) and 5 mg/kg DOX.

Metastases were induced in the PALN and lung by inoculation of tumor cells into the SiLN. Tumor cells in the lung were activated by resection of the SiLN

at 6 h post-inoculation (Shao, et al. 2015). Figure 4A (non-administration: control) shows metastases in the PALN and activated tumor cells in the lung on day 9 (after resection of the tumor-bearing SiLN at 6 h). DOX or DOX-LP alone was injected into the PALN at 6 h to treat tumor cells in the PALN and lung. Tumor cells in the PALN were inhibited; however, tumor cells in the lung were not inhibited. In contrast, DOX-LP+US inhibited tumor cells in both the PALN and lung.

Normalized luciferase activity in the PALN is shown in Fig. 4B. The treatment of tumor cells in the PALN with DOX-LP and US inhibited luciferase activity as compared with the non-administration, DOX alone or DOX-LP alone groups ($P < 0.05$: non-administration *vs* DOX-LP+US on day 6, non-administration *vs* DOX alone on day 6, non-administration *vs* DOX-LP+US on day 9).

Next, we examined the *ex vivo* luciferase activity of the lung at day 9 (Fig. 4C and Fig. 4D). Luciferase activity was detected in the non-administration, DOX alone and DOX-LP alone groups but not in the DOX-LP+US group ($P < 0.05$: non-administration *vs* DOX-LP alone, DOX alone *vs* DOX-LP alone; $P < 0.01$: non-administration *vs* DOX-LP+US, DOX alone *vs* DOX-LP+US).

Figure 5 shows representative images of the PALN and lung stained with HE and anti-CD31 antibody. Tumor cells were detected in the PALN of the non-administration group (Fig. 5A and Fig. 5B), but there was less metastasis in the DOX-LP+US group (0.48 W/cm^2) (Fig. 5C and Fig. 5D). In the lung, the non-administration group showed extravasation of tumor cells from the pulmonary arteries into the pulmonary parenchyma (Fig. 5E and Fig. 5F), while fewer tumor foci were detected in the DOX-LP+US group (Fig. 5G and Fig. 5H).

Discussion

The risk of recurrence following surgical resection of a primary tumor has been studied in clinical and animal experiments (Blezinger, et al. 1999, Dillekas, et al. 2016, Fisher, et al. 1989, Van Dierendonck, et al. 1991). White and colleagues reported that lung metastasis was induced by LN dissection (White, et al. 2002). We developed a mouse model of lung metastasis activation using MXH10/Mo/lpr mice, in which tumor cells in the lung are activated by resection of a tumor-bearing LN (Shao, et al. 2015). Although the mechanism of activation is still not well understood, it has been suggested that the primary tumor produces inhibitors of angiogenesis that circulate in the blood and suppress tumor growth in distant metastases (Peeters, et al. 2006).

In the present study, we aimed to develop a superselective drug delivery system using DOX-LP and US that could be used to treat lung metastases in a mouse model of lung metastasis activation. In mice, the efferent lymphatic vessel from the PALN is connected to the subclavian vein. Intranodal venules in the PALN are connected to the thoracoepigastric vein, which in turn is connected to the subclavian vein (Shao, et al. 2015, Takeda, et al. 2017). We have demonstrated that DOX-LP has a longer retention time in the LN than DOX alone due to the size of the particle (Moghimi and Moghimi 2008) and that US has the potential to permeabilize the lymphatic sinus and intranodal venules, resulting in the delivery of DOX into cells in the LN (Kato, et al. 2015, Kato, et al. 2015, Sato, et al. 2014, Sato, et al. 2015). Thus, DOX would be delivered from the axillary LNs to the metastatic lung via the subclavian vein, heart and pulmonary artery, resulting in a high anti-tumor effect in the lung (Fig. 4C).

In the present study, an US intensity (I_{SPTA}) of 0.48 W/cm^2 increased ICG retention in the PALN to a greater extent than an I_{SPTA} of 2.95 W/cm^2 (Fig. 2). This finding suggests that mild collapse of ICG-encapsulated liposomes may enhance the retention of ICG in the PALN. Since thermal effects on the release and retention of ICG in the PALN may be ignored (Draper and Ricard 1995), it is hypothesized that non-thermal mechanisms such as the formation of cavitation bubbles are involved (Miller, et al. 2012).

In our previous study (Kato, et al. 2015), DOX (at a concentration of 5 mg/kg body weight) was injected into the SiLN or tail vein to deliver it to the tumor-bearing PALN. Histological analysis revealed that the blood vessel lumens were smaller in the DOX alone (SiLN) group than in the PBS and DOX alone (tail vein) groups. The volume of the PALN decreased over time in the DOX alone (SiLN) and DOX alone (tail vein) groups compared with the PBS injection group, and body weight was significantly lower in the DOX alone (tail vein) group than in the PBS group. In our study, the concentration of DOX encapsulated in liposomes and injected into the SiLN was 1.25 mg/kg; comparable morphological, volume and body weight changes to those in our previous study were likely to have occurred.

Various liposome-modified drugs have been developed for the treatment of lung metastasis including lung-targeted docetaxel liposomes (Wang, et al. 2017) and paclitaxel-loaded pH-sensitive liposomes (Zhang, et al. 2016). The combination of our superselective drug delivery system with novel liposomes and US may overcome some of the limitations of current drug delivery methods (such as a rapid drug absorption by the recticulo-endothelial system in the liver and spleen, short circulation time and insufficient dosages at target sites) as well as reduce adverse

effects and increase the therapeutic index. The anti-tumor effects may be further improved by the use of a combination of nano/microbubbles and US, which further increases the permeability of the lymphatic sinus and intranodal veins (Kato, et al. 2015, Kato, et al. 2015, Sato, et al. 2014, Sato, et al. 2015).

The superselective drug delivery system described in this study could be used for drug screening to develop novel drugs for the treatment of lung cancer (Polley, et al. 2016, Wang, et al. 2017) and to investigate the mechanisms of tumor cell activation after resection of a primary tumor or LNs (Manjili 2017). The novel methodology and findings should prove highly useful for the future development of new chemotherapy techniques to treat lung metastasis, thereby improving the management of this serious cancer in patients.

Acknowledgements

The authors thank T. Sato for technical assistance and the Biomedical Research Core of Tohoku University Graduate School of Medicine for technical support. This study was supported in part by JSPS KAKENHI Grant Numbers 25293382 (MS), 15K15690 (MS), 16K15816 (SM), 26293425 (SM), 17K20077 (TK) and 17H00865 (TK).

References

Blezinger P, Wang J, Gondo M, Quezada A, Mehrens D, French M, Singhal A, Sullivan S, Rolland A, Ralston R, Min W. Systemic inhibition of tumor growth and tumor metastases by intramuscular administration of the endostatin gene. Nat. Biotechnol. 1999; 17:343-8.

Braunschweiger PG, Ting HL, Schiffer LM. Receptor-dependent antiproliferative effects of corticosteroids in radiation-induced fibrosarcomas and implications for sequential therapy. Cancer Res. 1982; 42:1686-91.

Demicheli R, Retsky MW, Hrushesky WJ, Baum M, Gukas ID. The effects of surgery on tumor growth: a century of investigations. Ann. Oncol. 2008; 19:1821-8.

Dillekas H, Demicheli R, Ardoino I, Jensen SA, Biganzoli E, Straume O. The recurrence pattern following delayed breast reconstruction after mastectomy for breast cancer suggests a systemic effect of surgery on occult dormant micrometastases. Breast Cancer Res. Treat. 2016; 158:169-78.

Draper DO, Ricard MD. Rate of temperature decay in human muscle following 3 MHz ultrasound: the stretching window revealed. J. Athl. Train. 1995; 30:304-7.

Fisher B, Gunduz N, Coyle J, Rudock C, Saffer E. Presence of a growth-stimulating factor in serum following primary tumor removal in mice. Cancer Res. 1989; 49:1996-2001.

Fritze A, Hens F, Kimpfler A, Schubert R, Peschka-Suss R. Remote loading of doxorubicin into liposomes driven by a transmembrane phosphate gradient. Biochim. Biophys. Acta 2006; 1758:1633-40.

Kato S, Mori S, Kodama T. A novel treatment method for lymph node metastasis using a lymphatic drug delivery system with nano/microbubbles and ultrasound. J. Cancer 2015; 6:1282-94.

Kato S, Shirai Y, Kanzaki H, Sakamoto M, Mori S, Kodama T. Delivery of molecules to the lymph node via lymphatic vessels using ultrasound and nano/microbubbles. Ultrasound Med. Biol. 2015; 41:1411-21.

Kodama T, Tomita Y, Koshiyama K, Blomley MJ. Transfection effect of microbubbles on cells in superposed ultrasound waves and behavior of cavitation bubble. Ultrasound Med. Biol. 2006; 32:905-14.

Li L, Mori S, Kodama M, Sakamoto M, Takahashi S, Kodama T. Enhanced sonographic imaging to diagnose lymph node metastasis: importance of blood vessel volume and density. Cancer Res. 2013; 73:2082-92.

Li L, Mori S, Sakamoto M, Takahashi S, Kodama T. Mouse model of lymph node metastasis via afferent lymphatic vessels for development of imaging modalities. PloS One 2013; 8:e55797.

Maniwa Y, Okada M, Ishii N, Kiyooka K. Vascular endothelial growth factor increased by pulmonary surgery accelerates the growth of micrometastases in metastatic lung cancer. Chest 1998; 114:1668-75.

Manjili MH. Tumor dormancy and relapse: from a natural byproduct of evolution to a disease state. Cancer Res. 2017; 77:2564-69.

Matsuki D, Adewale O, Horie S, Okajima J, Komiya A, Oluwafemi O, Maruyama S, Mori S, Kodama T. Treatment of tumor in lymph nodes using near-infrared laser light-activated thermosensitive liposome-encapsulated doxorubicin and gold nanorods. J. Biophotonics 2017; 10:1676-82.

Mikada M, Sukhbaatar A, Miura Y, Horie S, Sakamoto M, Mori S, Kodama T. Evaluation of the enhanced permeability and retention effect in the early stages of lymph node metastasis. Cancer Sci. 2017; 108:846-52.

Miller DL, Smith NB, Bailey MR, Czarnota GJ, Hynynen K, Makin IR, Bioeffects Committee of the American Institute of Ultrasound in Medicine. Overview of therapeutic ultrasound applications and safety considerations. J. Ultrasound Med. 2012; 31:623-34.

Miura Y, Mikada M, Ouchi T, Horie S, Takeda K, Yamaki T, Sakamoto M, Mori S, Kodama T. Early diagnosis of lymph node metastasis: importance of intranodal pressures. Cancer Sci. 2016; 107:224-32.

Moghimi SM, Moghimi M. Enhanced lymph node retention of subcutaneously injected IgG1-PEG2000-liposomes through pentameric IgM antibody-mediated vesicular aggregation. Biochim. Biophys. Acta 2008; 1778:51-5.

Peeters CF, de Waal RM, Wobbes T, Westphal JR, Ruers TJ. Outgrowth of human liver metastases after resection of the primary colorectal tumor: a shift in the balance between apoptosis and proliferation. Int. J. Cancer 2006; 119:1249-53.

Polley E, Kunkel M, Evans D, Silvers T, Delosh R, Laudeman J, Ogle C, Reinhart R, Selby M, Connelly J, Harris E, Fer N, Sonkin D, Kaur G, Monks A, Malik S, Morris J, Teicher BA. Small cell lung cancer screen of oncology drugs, investigational agents, and gene and microRNA expression. J. Natl. Cancer Inst. 2016; 108:djw122.

Sano K, Nakajima T, Choyke PL, Kobayashi H. Markedly enhanced permeability and retention effects induced by photo-immunotherapy of tumors. ACS Nano 2013; 7:717-24.

Sato T, Mori S, Arai Y, Kodama T. The combination of intralymphatic chemotherapy with ultrasound and nano-/microbubbles is efficient in the treatment of experimental tumors in mouse lymph nodes. Ultrasound Med. Biol. 2014; 40:1237-49.

Sato T, Mori S, Sakamoto M, Arai Y, Kodama T. Direct delivery of a cytotoxic anticancer agent into the metastatic lymph node using nano/microbubbles and ultrasound. PloS One 2015; 10:e0123619.

Shao L, Mori S, Yagishita Y, Okuno T, Hatakeyama Y, Sato T, Kodama T. Lymphatic mapping of mice with systemic lymphoproliferative disorder: usefulness as an inter-lymph node metastasis model of cancer. J. Immunol. Methods 2013; 389:69-78.

Shao L, Ouchi T, Sakamoto M, Mori S, Kodama T. Activation of latent metastases in the lung after resection of a metastatic lymph node in a lymph node metastasis mouse model. Biochem. Biophys. Res. Commun. 2015; 460:543-8.

Shao L, Takeda K, Kato S, Mori S, Kodama T. Communication between lymphatic and venous systems in mice. J. Immunol. Methods 2015; 424:100-5.

Tagliabue E, Agresti R, Carcangiu ML, Ghirelli C, Morelli D, Campiglio M, Martel M, Giovanazzi R, Greco M, Balsari A, Menard S. Role of HER2 in wound-induced breast carcinoma proliferation. Lancet 2003; 362:527-33.

Takeda K, Mori S, Kodama T. Study of fluid dynamics reveals direct communications between lymphatic vessels and venous blood vessels at lymph nodes of mice. J. Immunol. Methods 2017; 445:1-9.

Van Dierendonck JH, Keijzer R, Cornelisse CJ, Van de Velde CJ. Surgically induced cytokinetic responses in experimental rat mammary tumor models. Cancer 1991; 68:759-67.

Wang DC, Wang W, Zhu B, Wang X. Lung cancer heterogeneity and new strategies for drug therapy. Annu. Rev. Pharmacol. Toxicol. 2018; 58:531-546.

Wang L, Li R, Che K, Liu Z, Xiang S, Li M, Yu Y. Enhanced antitumor effect on intrapulmonary tumors of docetaxel lung-targeted liposomes in a rabbit model of VX2 orthotopic lung cancer. Sci. Rep. 2017; 7:10069.

White RR, Stanley WE, Johnson JL, Tyler DS, Seigler HF. Long-term survival in 2,505 patients with melanoma with regional lymph node metastasis. Ann. Surg. 2002; 235:879-87.

Zhang L, Wang Y, Xia T, Yu Q, Zhang Q, Yang Y, Cun X, Lu L, Gao H, Zhang Z, He Q. Suppression for lung metastasis by depletion of collagen I and lysyl oxidase via losartan assisted with paclitaxel-loaded pH-sensitive liposomes in breast cancer. Drug Deliv. 2016; 23:2970-79.

Figure legends

Figure 1. Experimental procedure.

(A) Lymphatic and vascular system in MXH10/Mo/lpr mice (Takeda, et al. 2017). The efferent lymphatic vessel of the PALN is connected to the subclavian vein (Shao, et al. 2013). The thoracoepigastric vein runs adjacent to the SiLN and PALN and connects to the inferior vena cava and subclavian vein. PALN: proper axillary lymph node, SiLN: subiliac lymph node.

(B) Induction of metastasis in the PALN. The area between the SiLN and PALN was clamped to prevent flow from the SiLN to the PALN via lymphatic vessels and the thoracoepigastric vein. Cells were manually injected into the middle of the SiLN through an incision.

(C) Injection of DOX or DOX-LP into the SiLN. At 6 h post-inoculation of tumor cells, DOX alone or DOX-LP was injected into the PALN under US guidance at a rate of 50 μL/min using a syringe pump.

(D) Delivery of DOX to the lung and activation of metastatic tumor cells in the lung. The PALN was exposed to 1-MHz US. A bipolar coagulator and surgical microscope were used to facilitate the SiLN resection process. After excision of the SiLN, the surgical area was thoroughly washed with saline to remove any tumor cells that had leaked from the tumor-bearing SiLN. The skin wound was closed with sutures.

Figure 2. *In vivo* fluorescence intensity of the PALN

(A) *In vivo* monitoring of ICG, ICG-LP1 and ICG-LP2 fluorescence at various time points. ICG solution (n = 3), ICG-LP1 (n = 3) or ICG-LP2 (n = 3) were injected into the PALN at a rate of 50 μL/min for 2 min. ICG solution had spread from the PALN to the liver at 30 min after injection, and fluorescence in the PALN was not detected at 48 h after injection. ICG-LP1 had spread from the PALN to the liver at 30 min after injection, and fluorescence in the PALN was decreased at 48 h after injection. ICG-LP2 also spread from the PALN, but signals in the liver were not detected until after 1 h. Strong fluorescence intensity was detected in the PALN at 48 h after injection, as compared with ICG-LP1.

(B) *In vivo* monitoring of ICG-LP2 fluorescence after exposure to US. ICG-LP2 solution was injected into the PALN at a rate of 50 μL/min for 2 min. The PALN was exposed to US (2.95 W/cm^2, n = 3 or 0.48 W/cm^2, n = 3) 30 min after the injection.

(C) Fluorescence intensity of ICG, ICG-LP1 or ICG-LP2, with and without exposure to US, in the PALN (as shown in A and B). ICG and ICG-LP1 reached peak fluorescence intensity at 1 h after injection, while ICG-LP2 fluorescence peaked at 3 h after injection (i.e., ICG-LP2 was better retained in the PALN than ICG or ICG-LP1). The fluorescence intensity of ICG-LP2 after exposure to US increased rapidly at 30 min, peaked at 1 h and then rapidly decreased. ICG (n = 3), ICG-LP1 (n = 3), ICG-LP2 (n = 3), ICG-LP2 + 0.48 W/cm^2 (n = 3), ICG-LP2 + 2.95 W/cm^2 (n = 3).

Figure 3. *Ex vivo* fluorescence intensity in various organs

Mice were treated under the conditions shown in Fig. 2. Mice were sacrificed at 48 h, and various organs (liver, lungs, heart, PALN) were removed. The ICG fluorescence intensity in the PALN was higher for ICG-LP2 exposed to US at 0.48 W/cm^2 than for ICG-LP2 exposed to US at 2.95 W/cm^2. This indicates that US at 0.48 W/cm^2 released more ICG from ICG-LP2 than US at 2.95 W/cm^2. ICG (n = 3), ICG-LP1 (n = 3), ICG-LP2 (n = 3), ICG-LP2 + 0.48 W/cm^2 (n = 3), ICG-LP2 + 2.95 W/cm^2 (n = 3). *P < 0.05, **P < 0.01, post-hoc Tukey-Kramer test.

Figure 4. Antitumor effect of DOX-LP and US in the PALN and lung

Tumor cells were inoculated into the SiLN. DOX-LP (466.8 ± 44.3 nm) was injected into the PALN at 6 h post-inoculation, and the PALN was then exposed to US (0.48 W/cm^2). The SiLN was resected to activate lung metastasis.

(A) Bioluminescence imaging on day 9 post-inoculation. For the non-administration (control) group, luciferase activity was detected in the PALN and lung. In both the DOX alone and DOX-LP alone groups, luciferase activity was detected in the lung. For the DOX-LP+US group, luciferase activity was not detected in either the PALN or lung. Non-administration (n = 4), DOX alone (n = 4), DOX-LP alone (n = 4), DOX-LP+US (0.48 W/cm^2) (n = 4).

(B) Changes in luciferase activity in the PALN with time, as shown in (A). The values in each group were normalized to that at 6 h post-inoculation. The luciferase activity increased with time in the non-administration (control) and DOX alone groups. The luciferase activity increased to a smaller extent in the DOX-LP group and remained at background levels in the DOX-LP+US group. *P < 0.05 (Mann-Whitney U test): non-administration *vs* DOX-LP+US on day 6;

non-administration *vs* DOX alone on day 6; non-administration *vs* DOX-LP+US on day 9. Non-administration (n = 4), DOX alone (n = 4), DOX-LP alone (n = 4), DOX-LP+US (0.48 W/cm^2) (n = 4).

(C) *Ex vivo* bioluminescence imaging of the lungs on day 9 post-inoculation, following the experiments shown in (A). Bioluminescence signals were detected in the entire lungs in the non-administration and DOX alone groups. Reduced bioluminescence signals were detected in the lungs in the DOX-LP alone group. Bioluminescence signals were not detected in the lungs in the DOX-LP+US (0.48 W/cm^2) group. Non-administration (n = 4), DOX alone (n = 4), DOX-LP alone (n = 4), DOX-LP+US (0.48 W/cm^2) (n = 4).

(D) *Ex vivo* luciferase activity of lungs removed on day 9 post-inoculation, as shown in (C). The values were normalized to the mean value of the non-administration group. Normalized luciferase activity in the DOX alone group was similar to that of the non-administration (control) group, but luciferase activity in the DOX-LP alone group was reduced by about 50%. Fluorescence activity in the DOX-LP+US group was decreased to the background level. Non-administration (n = 4), DOX alone (n = 4), DOX-LP alone (n = 4), DOX-LP+US (0.48 W/cm^2) (n = 4). *P < 0.05 (Steel-Dwass test): non-administration *vs* DOX-LP alone, DOX alone *vs* DOX-LP alone; **P < 0.01 (Steel-Dwass test): non-administration *vs* DOX-LP+US, DOX alone *vs* DOX-LP+US.

Figure 5. Histological analysis of the PALN and lung

A–D: PALN. A, C: HE staining; B, D: anti-CD31 staining. Metastatic foci were detected in the entire PALN in the non-administration (control) group (A and B),

while metastatic foci were not detected in the PALN in the DOX-LP+US group (C and D). meta: metastasis; arrowheads: endothelium. Scale bar: 50 μm.

E–H: Lung. E, G: HE staining; F, H: anti-CD31 staining. Metastatic foci were detected within and outside intranodal venules in the non-administration (control) group (E and F). There were fewer metastatic foci in the DOX-LP+US group than in controls. meta: metastasis; arrowheads: endothelium. Scale bar: 200 μm.

Appendices

Figure A.1. Release of ICG and DOX from liposomes

(A) Release of ICG from ICG-LP at 37°C. ICG-LP (320 nm in diameter). Release of ICG from both ICG-LP was detected at 6 h after inoculation. The release ratio was 40%. The absorbance was measured at 800 nm. Samples (n = 1) at each time. (B) Release of DOX from DOX-LP at 37°C. A sudden release of DOX was detected at 6 h, yet 80% of DOX-LP remained stable (0 h versus 6 h, 0 h versus 24 h, 0 h versus 48 h, $^{**}P < 0.01$, post-hoc Bonferroni test). The absorbance was measured at 480 nm. Samples (n = 3) at each time point. Both (A) and (B) indicate that ICG-LP and DOX-LP have similar release characteristics.

Table 1. Characteristics of ICG- and DOX-encapsulated liposomes

	ICG-LP1 (n = 2)	ICG-LP2 (n = 3)	DOX-LP (n = 4)
Lipid composition	DSPC:DSPE-PEG = 94:6	DSPC:DSPE-PEG = 94:6	DSPC:DSPE-PEG = 94:6
Encapsulated drug	ICG	ICG	DOX
Diameter (nm)	134.7 ± 9.39	462.3 ± 87.6	466.8 ± 44.3
Zeta potential (mV)	-1.08 ± 0.36	-1.25 ± 0.50	-0.83 ± 0.61
Encapsulation efficiency (%)	-	-	69.3 ± 13.1

Data are shown as the mean ± standard deviation. DOX: doxorubicin; DSPC: 1,2-distearoyl-sn-glycero-3-phosphatidylcholine; DSPE-PEG: 1,2-distearoyl-sn-glycerol-3-phosphatidylethanolamine-methoxy-polyethylenglycol; ICG: indocyanine green; LP: liposomes.

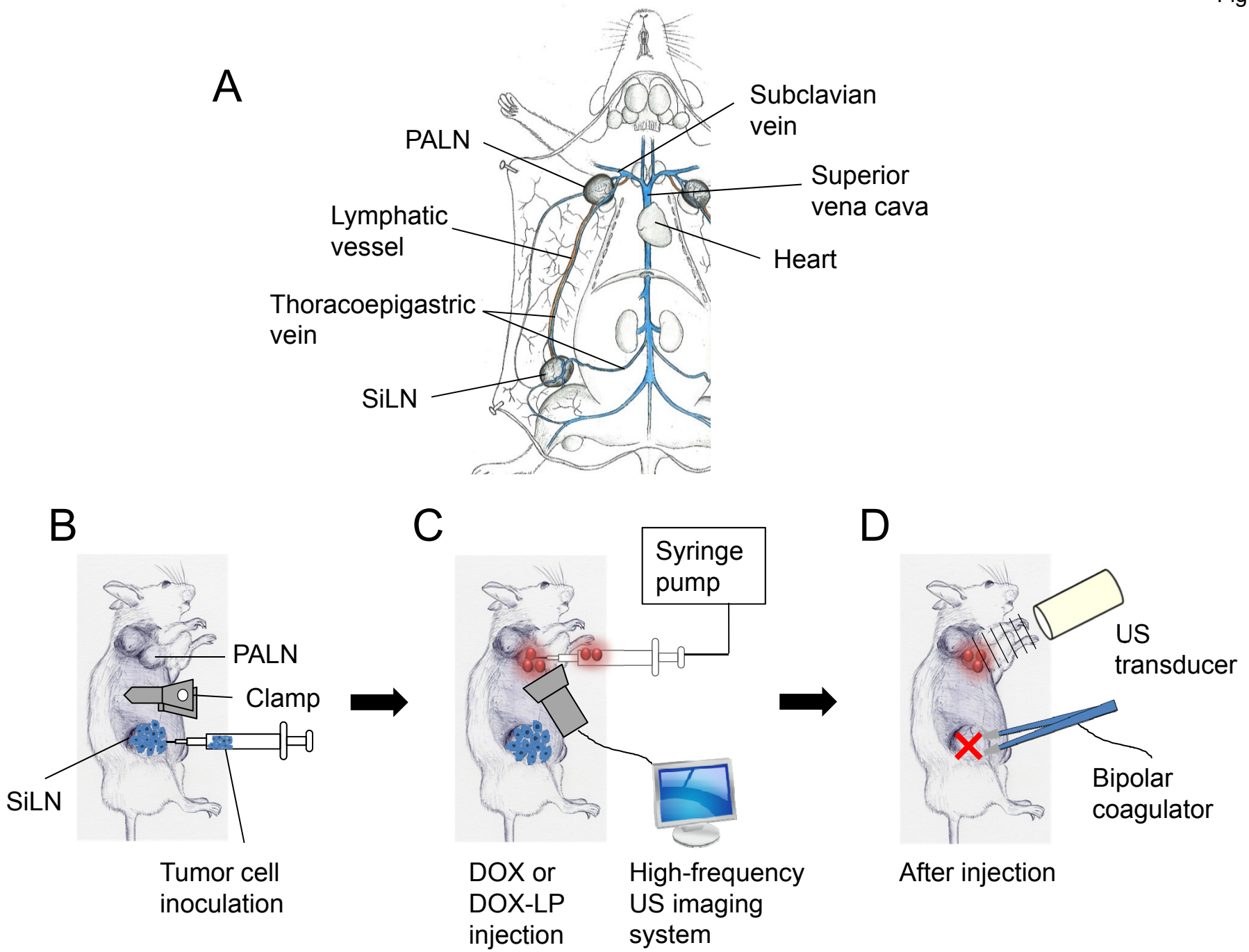
A
Subclavian vein
PALN
Superior vena cava
Lymphatic vessel
Heart
Thoracoepigastric vein
SiLN
B
PALN
Clamp
SiLN
Tumor cell inoculation
C
Syringe pump
DOX or DOX-LP injection
High-frequency US imaging system
D
US transducer
Bipolar coagulator
After injection

Fig. 2

A

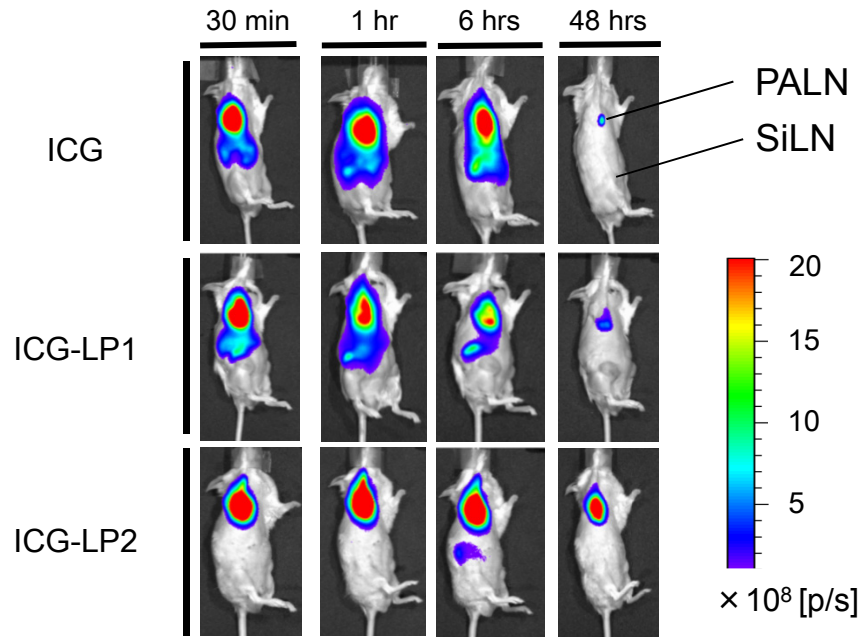
30 min
1 hr
6 hrs
48 hrs
ICG
ICG-LP1
ICG-LP2
PALN
SiLN
20
15
10
5
× 10⁸ [p/s]

B

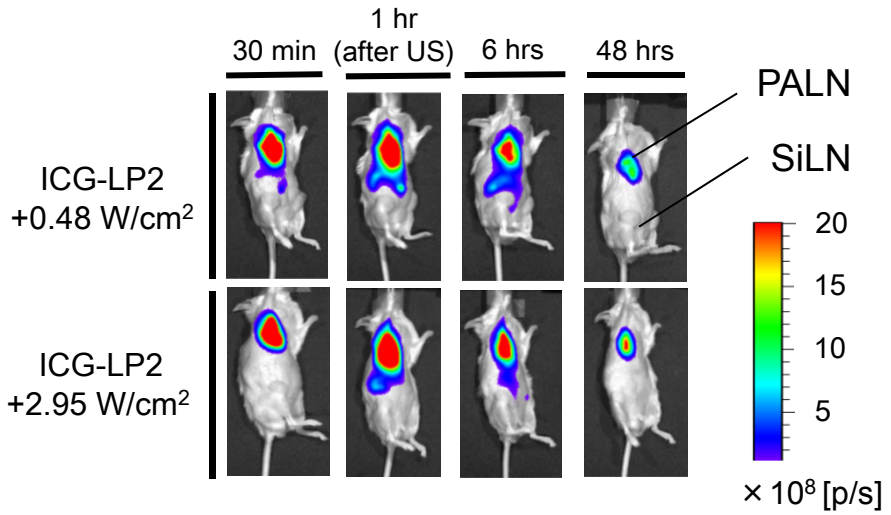
30 min
1 hr
(after US)
6 hrs
48 hrs
ICG-LP2
+0.48 W/cm²
ICG-LP2
+2.95 W/cm²
PALN
SiLN
20
15
10
5
× 10⁸ [p/s]

C

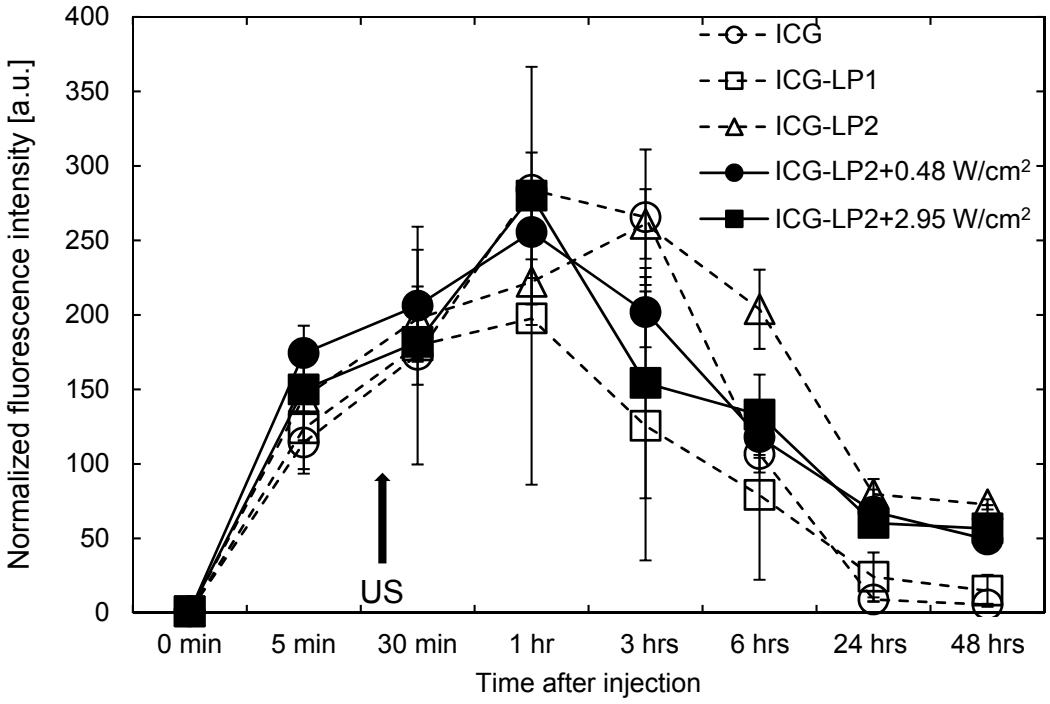
Normalized fluorescence intensity [a.u.]
400
350
300
250
200
150
100
50
0
US
0 min
5 min
30 min
1 hr
3 hrs
6 hrs
24 hrs
48 hrs
Time after injection
ICG
ICG-LP1
ICG-LP2
ICG-LP2+0.48 W/cm²
ICG-LP2+2.95 W/cm²

Fig. 3

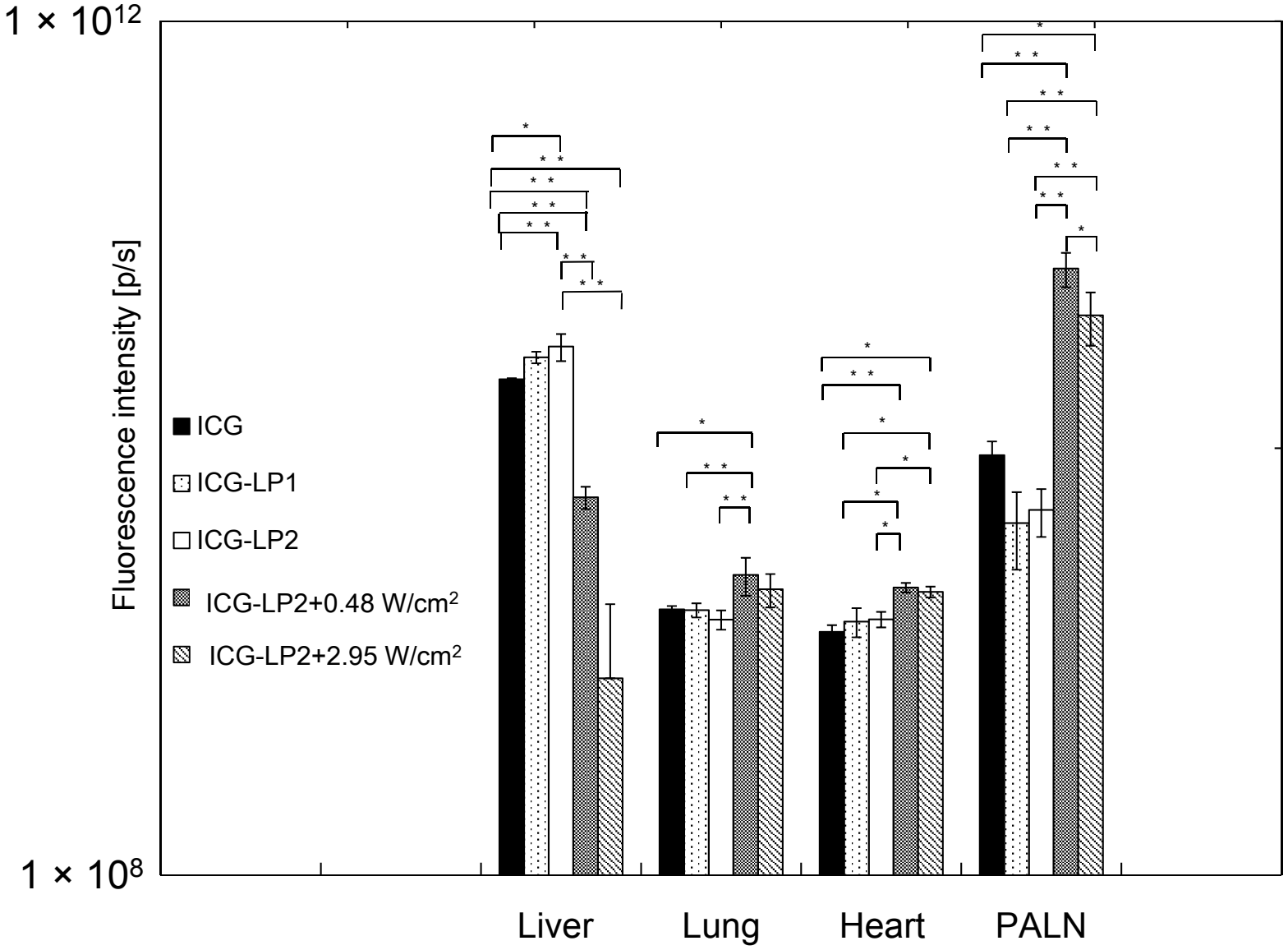
1 × 10^12
1 × 10^8
Fluorescence intensity [p/s]
ICG
ICG-LP1
ICG-LP2
ICG-LP2+0.48 W/cm2
ICG-LP2+2.95 W/cm2
Liver
Lung
Heart
PALN

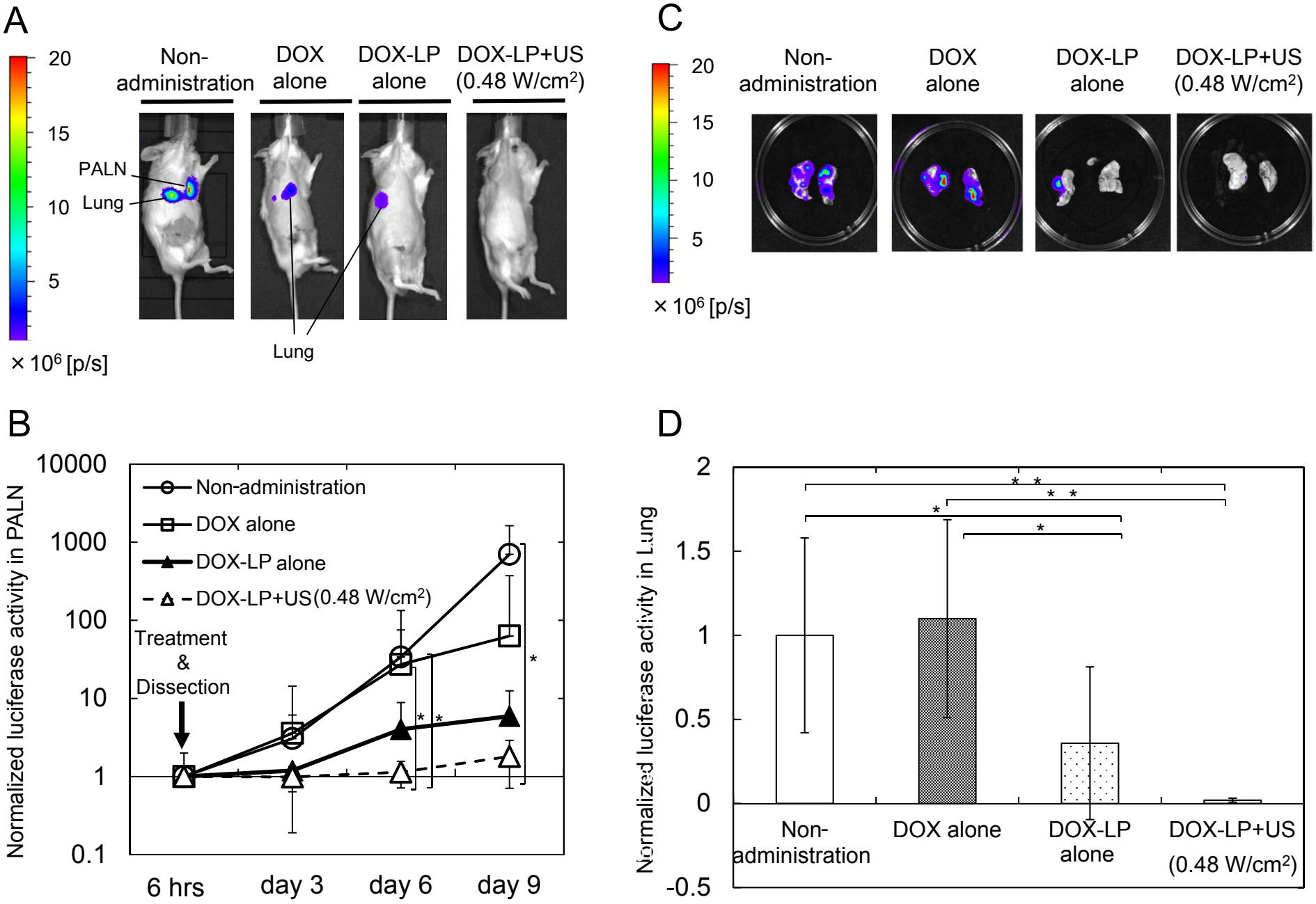
A
20
15
10
5
× 10⁶ [p/s]
Non-administration
DOX alone
DOX-LP alone
DOX-LP+US (0.48 W/cm²)
PALN
Lung
Lung
C
20
15
10
5
× 10⁶ [p/s]
Non-administration
DOX alone
DOX-LP alone
DOX-LP+US (0.48 W/cm²)
B
Normalized luciferase activity in PALN
10000
1000
100
10
1
0.1
Non-administration
DOX alone
DOX-LP alone
DOX-LP+US(0.48 W/cm²)
Treatment
&
Dissection
6 hrs
day 3
day 6
day 9
D
Normalized luciferase activity in Lung
2
1.5
1
0.5
0
-0.5
Non-administration
DOX alone
DOX-LP alone
DOX-LP+US (0.48 W/cm²)

Fig. 5

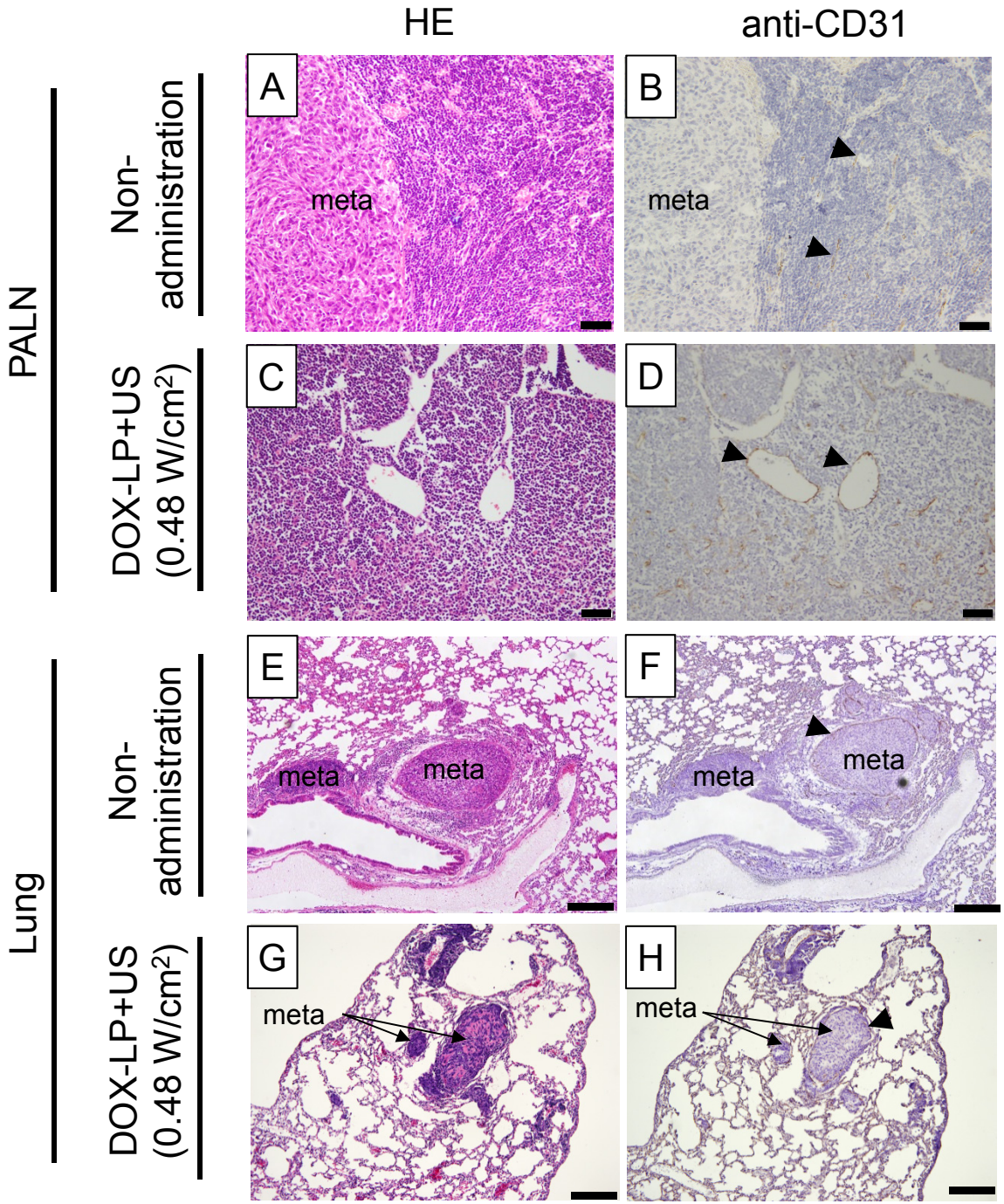
HE
anti-CD31
PALN
Non-administration
DOX-LP+US (0.48 W/cm²)
Lung
Non-administration
DOX-LP+US (0.48 W/cm²)
A
B
C
D
E
F
G
H
meta

Fig. A.1

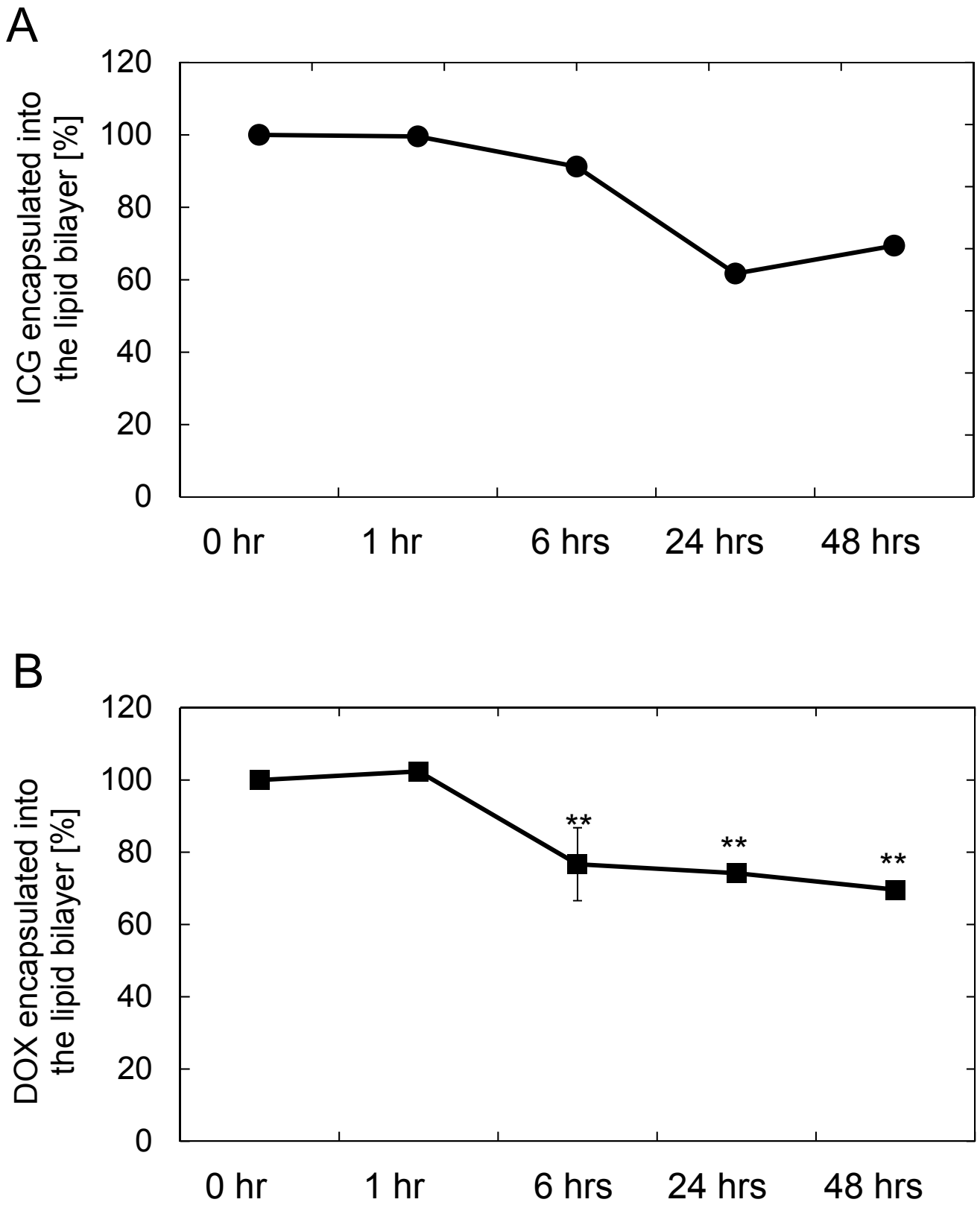
A
ICG encapsulated into the lipid bilayer [%]
120
100
80
60
40
20
0
0 hr
1 hr
6 hrs
24 hrs
48 hrs
B
DOX encapsulated into the lipid bilayer [%]
120
100
80
60
40
20
0
**
**
**
0 hr
1 hr
6 hrs
24 hrs
48 hrs